ELSEVIER

Ultrasonics 40 (2002) 385–392

Ultrasonics

www.elsevier.com/locate/ultras

Modelling of layered resonators for ultrasonic separation

Martyn Hill [a,*], Yijun Shen [a], Jeremy J. Hawkes [b]

[a] School of Engineering Sciences, University of Southampton, Highfield, Southampton, SO17 1BJ, UK
[b] Cardiff School of Biosciences, P.O. Box 911, Cardiff CF10 3US, UK

Abstract

The potential of ultrasonic techniques for the separation and concentration of particles within a fluid has been investigated in some detail in recent years. Devices for effecting such separation typically consist of a piezoceramic transducer driving into a matching layer, fluid layer and reflector layer.

This paper uses an equivalent-circuit transducer model, coupled with acoustic impedance transfer relationships to model such cells with regards to both their electrical characteristics and the strength of the resonance produced under different conditions. The model is compared with experimental results from two different cells and is shown to match experimental values well in terms of electrical characteristics and separator performance. The effects of matching layer thickness are also examined using the model.

The importance of the adhesive bonding layer is demonstrated, and it is shown that the model can predict the effects of such a layer. The model is also used to demonstrate the effects of coincident resonances in cell layers and to examine the pressure distribution across cells at key frequencies.

Keywords: Layered resonators; Ultrasonic separation; Computer modelling

1. Introduction

High frequency acoustic standing waves can be used to concentrate particles (or a second fluid phase) at nodal, or antinodal planes within a fluid [1–3]. The phenomenon can be used amongst other things to agglomerate particles, to trap particles within a flow, or to filter or concentrate particles within that flow.

Typically, systems for achieving ultrasonic separation are based on a layered resonator. In such a resonator a piezoelectric transducer is bonded to a carrier or matching layer which in turn drives a fluid layer (in which the separation takes place) and which is terminated by a reflector layer. The dimensions and properties of these layers have a profound influence on the performance of the cell. This paper describes a model which is being used to help understand the influence of geometric and material design parameters on behaviour of a layered resonator used for ultrasonic separation. Following a brief description of the model itself, a comparison of modelled predictions and experimental results is presented. Results of numerical experiments in which design parameters are varied are discussed and used to explain aspects of the resonator's behaviour.

2. Theory

2.1. Structure of separation cell

A schematic diagram of a typical ultrasonic separation cell is shown in Fig. 1. It consists of a piezoceramic transducer driving into a matching layer, fluid layer and reflector layer.

The piezoelectric layer is driven as a thickness (d_{33}) transducer, although not necessarily at one of its thickness resonances. The acoustic energy is often (though not invariably) transmitted to the fluid layer via a matching layer. The function of the matching layer (along with its design parameters) when driving into the acoustic free-field are well understood, and in such a case the layer acts to match the high acoustic impedance transducer to the low acoustic impedance of the water. When driving into an enclosure however, particularly when that enclosure has little damping, the acoustic

* Corresponding author. Tel.: +44-23-8059-3075; fax: +44-23-8059-3053.
E-mail address: m.hill@soton.ac.uk (M. Hill).

0041-624X/02/$ - see front matter
PII: S0041-624X(02)00127-0

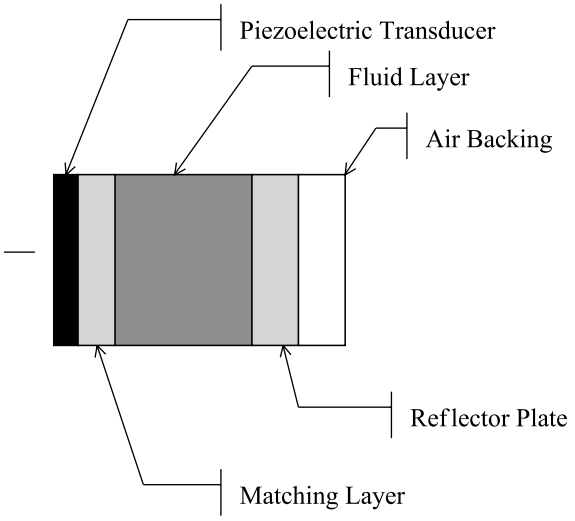

Fig. 1. Schematic diagram of the ultrasonic separation cell.

impedance presented by the fluid layer varies hugely with frequency and the importance of this layer is more complex. Indeed the primary purpose of this layer may be structural, or aimed at isolating the transducer from the fluid, rather than as an impedance matching layer.

The fluid layer, which will also contain the particles or second phase to be separated, must hold an ultrasonic standing wave, which controls the separation process, and to this end, the reflector plate must offer an impedance which reflects most of the acoustic energy back into the fluid layer.

2.2. Transducer and impedance transfer modelling

The equivalent-circuit transducer model, valid near the first thickness resonance of the transducer, is shown in Fig. 2 and is described in more detail by Hill and Wood [4] and Hill [5] (see Nowotny and Benes [6] for a more general formulation).

In this circuit, C_0 expresses the static capacitance of the transducer, C_m, L_m, and R_m denote the equivalent mechanical capacitance, inductance and resistance respectively, and Z_0 denotes the input impedance of the layered resonator. C_0, C_m and L_m can be determined through calculating the mechanical parameters of the transducer using the method described by Stansfield [7] and Hueter and Bolt [8]. The mechanical resistance R_m, along with other damping values within the system, are estimated experimentally.

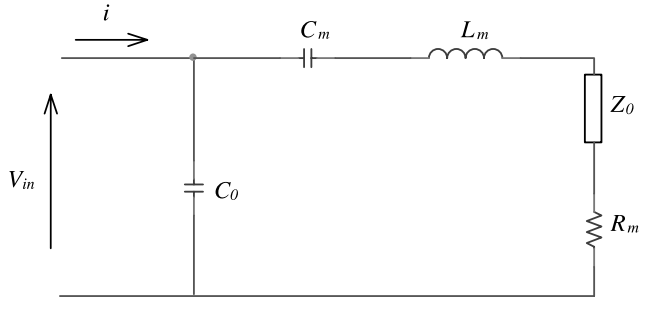

Fig. 2. Equivalent circuit of the transducer.

Assuming that the acoustical characteristics of the resonator are dominated by waves travelling in the thickness direction of the layers, the input mechanical impedance, Z_0, is given by Kinsler et al. ([9], Sections 9.2 and 6.3):

$$Z_0 = r_m S \frac{Z_f + j r_m S \tan k_m t_m}{r_m S + j Z_f \tan k_m t_m} \tag{1}$$

In the equation above, Z_0 is the input mechanical impedance to the matching layer. Z_f is the mechanical impedance looking in to the fluid layer. S and t_m are the cross-sectional area of the cavity and the thickness of the matching layer respectively. The specific acoustic impedance of the matching layer is r_m, and k_m denotes the wave number in that layer. The wave number is generally complex to allow for losses within the layer. Z_f can be calculated using the same impedance transfer relationship (Eq. (1)) for the liquid layer, and so on until an acoustic free field boundary is encountered, at which point the terminating impedance can be calculated from the specific acoustic impedance of the final medium (usually air).

3. Modelling of acoustic parameters within the cell

3.1. Acoustic pressure and velocity

The model derived above provides an estimate of the electrical impedance characteristics of the cell. In order to model the performance of the cell in more detail, it is also necessary to model the acoustic behaviour within the cell, and in particular within the liquid layer.

The force, F_0, generated by the transducer and acting on the matching layer can be shown to be ([7], Section 4.8)

$$F_0 = \frac{\varphi V Z_0}{Z_m + Z_0} \tag{2}$$

where, V is the input voltage, φ is a transformation ratio between electrical and mechanical quantities and Z_m is the mechanical impedance of the resonant transducer at the output terminals when the electrical terminals are short-circuited. This in turn generates a force, F_f, between the matching layer and the fluid which is given by

$$F_f = \frac{F_0 Z_f}{Z_f \cos k_m t_m + j r_m S \sin k_m t_m} \tag{3}$$

If there are multiple layers between the transducer and the fluid layer, the same force transfer relationship can be used on successive layers to calculate the force at the

fluid boundary. The input voltage, V, is derived from the electrical input impedance and a knowledge of the output impedance of the driving amplifier.

If the fluid layer has a thickness t_f and we let $x = 0$ at the matching layer/fluid boundary, then the spatial variation of the acoustic pressure, $p(x)$, through the fluid layer may be expressed as:

$$p(x) = \frac{F_f}{S} \frac{Z_r \cos k_f(t_f - x) + jr_f S \sin k_f(t_f - x)}{Z_r \cos k_f t_f + jr_f S \sin k_f t_f} \quad (4)$$

The corresponding relationship for acoustic velocity variation through the cell is

$$u(x) = \frac{F_f}{r_f S} \frac{r_f S \cos k_f(t_f - x) + jZ_r S \sin k_f(t_f - x)}{Z_r \cos k_f t_f + jr_f S \sin k_f t_f} \quad (5)$$

where r_f and k_f are the specific acoustic impedance and the wave number in the fluid layer, and Z_r is the mechanical impedance looking into the reflector layer.

3.2. Acoustic energy measures

From Kinsler et al. ([9], Section 5.8), the instantaneous energy density, ε_i, at a point within the standing wave field of a fluid of density ρ can be expressed as

$$\varepsilon_i(x) = \frac{1}{2}\rho\left(u(x)^2 + \frac{p(x)^2}{r_f^2}\right) \quad (6)$$

The time average of the instantaneous energy density $\langle \varepsilon_i(x) \rangle_t$ can be calculated using the real parts of pressure and velocity above. This can then be integrated numerically to calculate the total, time averaged, energy stored in the fluid layer:

$$E_f = S \int_0^{t_f} \langle \varepsilon_i(x) \rangle_t \, dx \quad (7)$$

The acoustic forces acting on a small spherical particle in a standing wave can be shown to be proportional to the product of the energy density in the standing wave and the driving frequency (see for example [10]). In this study the product of total energy and frequency ($E_f f$ J s^{-1}) is used as a prediction of filtration performance (note that while the product is dimensionally equivalent to power in Watts, it is labelled J s^{-1} to avoid confusion as it's a measure of stored rather than dissipated energy). This is only valid if a realistic model of the electrical source is included, as a pure voltage source will predict a performance that is unrealistic in most experimental situations. An alternative parameter that can be used to predict cell behaviour is the performance number defined by Gröschl [11]. This equals the stored energy E_f in the fluid divided the total energy lost in the resonator averaged over one oscillation period. This has been shown to be a very useful measure of resonator performance, particularly in filter design and the selection of appropriate working frequencies. However, it is essentially a measure of efficiency and as such is beyond the scope of this paper.

4. Experimental validation of the model

The model has been validated against experimental results taken from a variety of different ultrasonic separators with differing configurations and liquid layer sizes ranging from 0.25 mm up to about 50 mm. The following example compares model and experimental results for the *Laminar Flow Filter* described by Hawkes and Coakley [12].

4.1. The cardiff laminar flow filter

This continuous flow filter uses a long but very narrow liquid layer to ensure that the flow regime is laminar throughout the separation process. A schematic diagram of the layered resonator is shown in Fig. 3.

The exact thicknesses of the epoxy resin and silver electrodes were not known, and approximations have been used. Measurements of electrical input impedance for both empty and full cells were available, along with measurements of the cell's performance, in terms of the particle clearance effected by the cell.

4.2. Impedance modelling of the filter

4.2.1. Basic model

Using the model described above, and modelling the amplifier used by Hawkes and Coakley as providing 50 dB gain to a voltage source of 20 mV, with a 50 Ω output impedance, allows a comparison to made between the modelled and measured voltages across the transducer.

Fig. 4 shows modelled and measured voltages across the transducer when the cell is empty. In this case, only the transducer, electrode, epoxy and steel layers need to be modelled. Thickness values used in the model are

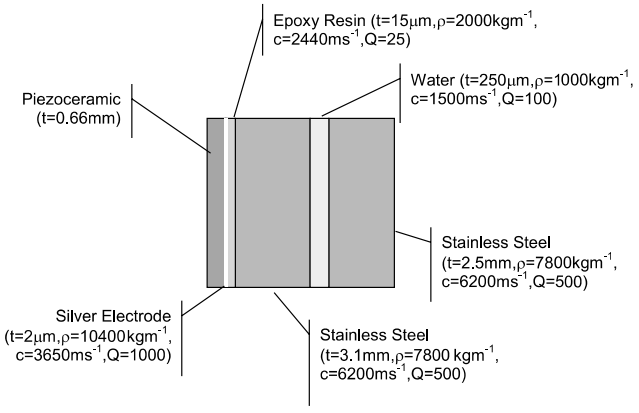

Fig. 3. Schematic diagram of Hawkes and Coakley's laminar flow filter. Not to scale.

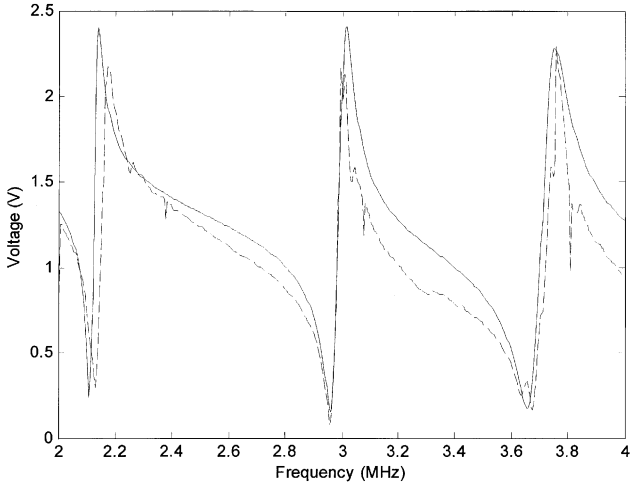

Fig. 4. Voltage across the ceramic for the empty cell. Experimental—dashed line, Modelled—solid line.

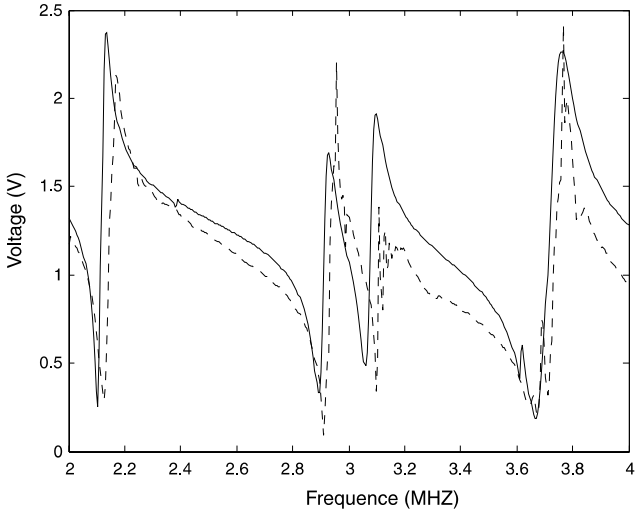

Fig. 5. Voltage across the ceramic for the full cell. Experimental—dashed line, Modelled—solid line.

taken from design data. Values of density and sonic velocity are taken from material data sheets or experimental measurements when available or published values for similar materials when not.

Losses in the model, represented by Q factors in each layer, are estimated empirically. These have not, to date, proved amenable to a priori estimates as the losses depend not only on the material parameters themselves, but also on the cell geometry and construction. It is also likely that any lack of flatness or parallelism between the faces will also appear to increase the system damping.

The overall forms of the voltage spectra match well (with modelled peaks at 2.14, 3.01, and 3.75 MHz and measured peaks at 2.18, 3.00, and 3.76 MHz). As the cell is air rather than water filled, the features shown are due entirely to the resonances of the transducer, silver, epoxy and steel layers.

Once appropriate loss parameters have been established, the remaining fluid and reflector layers can be added to the model, as shown in Fig. 5.

The frequencies of the peaks at about 2.1 and 3.7 MHz remain almost unchanged in both model and experiment. However, the central (~3 MHz) peak has been replaced by two peaks: one at a frequency lower than the original peak (2.92 MHz modelled, 2.95 MHz experimental) and one at a higher frequency (3.10 modelled and 3.11 MHz experimental). Both spectra now show a smaller peaks in the 3.6–3.7 MHz frequency range, and interestingly a feature has appeared in the modelled data at about 2.39 MHz which is not seen in this experimental spectrum, but may correspond to a similar feature at 2.38 MHz in the empty cell experimental spectrum.

The most striking differences between the spectra are the amplitudes and the detailed features in the 3.11 MHz resonance. This peak is likely to be due to the chamber itself and the differences could be due to an underestimate of damping, perhaps due to errors in flatness or parallelism. Fine details in the experimental results could be due to coupling with other modes, perhaps high lateral modes in the chamber

4.2.2. Effects of layer bonding

In the laminar flow device described above, a comparison of numerical simulations and experimental results suggests that the adhesive layer has only a relatively small effect on the modelled electrical characteristics. The authors assume that this is because the adhesive layer is thin and well bonded to the adjacent layers. This is not always the case however as can be seen from the three graphs shown in Fig. 6 in which a larger cell (20 mm cavity) of Hawkes and Coakley (called here the 20 mm cell) is modelled.

Fig. 6(a) shows modelled and experimental results for the 20 mm cell with no matching layer. The model provides a good representation of trends in the experimental detail throughout the frequency range for which experimental data was available (up to about 3.4 MHz).

Fig. 6(b) shows experimental results from the same cell, with the addition of a $3\lambda/2$ (at 3 MHz) aluminium matching layer, along with modelled results in which the matching layer is directly adjacent to the transducer. The low peak in the experimental results at about 2.2 MHz is replaced by a much higher peak at about 2.5 MHz. Both model and experiment show a peak at about 3.2 MHz, but the peak is much higher in the modelled results, and most noticeably, the large experimental peak at 3.5 MHz is completely missing from the modelled data.

Fig. 6(c) shows the same experimental results, but the model now includes an epoxy layer of 60 μm thickness between the transducer and the matching layer. The peaks at 2.2 and 3.5 MHz are now very well represented

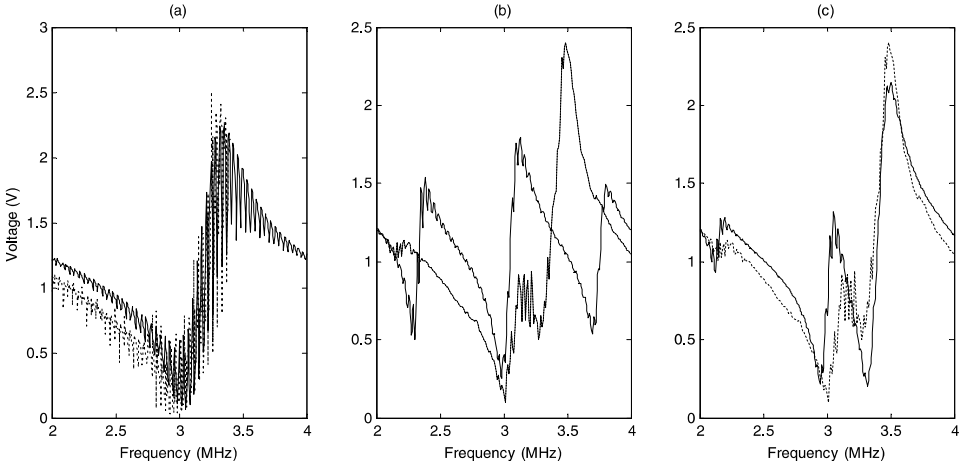

Fig. 6. Voltage across the ceramic for 20 mm cell. (a) cell with no matching layer, (b) cell with a matching layer included, (c) cell after the addition of an adhesive layer to the model. Experimental—dotted line, Modelled—solid line.

by the model and while the modelled central peak has now moved to about 3.1 MHz, its overall shape is much closer to the experimental results. From these results, the authors deduce that the adhesive layer is only poorly bonded in this particular device.

4.3. Acoustical modelling of the filter

4.3.1. Energy and clearance

Data for the filtration efficiency is available for the laminar-flow cell, in terms of the clearance of particles from the clean outlet. Fig. 7 shows a comparison of measured clearance due to the filter and the predicted performance in terms of the energy–frequency product.

The model clearly predicts the two clearance peaks, and while the match is not exact in terms of peak centre frequency and the relative height of the two peaks, the form of the graph provides a good match. Once more, the model does not predict the fine detail that is visible in the experimental results, which may again be due to modal coupling.

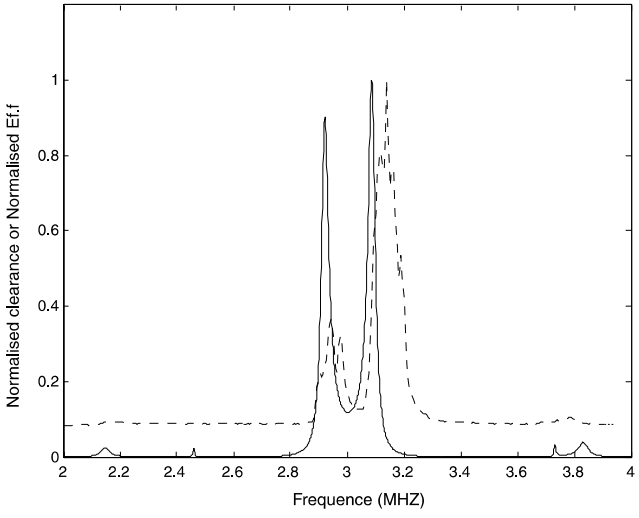

Fig. 7. Comparison of measured clearance—dashed line, and modelled energy–frequency product—solid line.

5. Parametric studies using the resonator model

Having demonstrated that the model provides a reasonable approximation to measured data, it is possible to use the model to examine details of resonator behaviour and predict the effects of parameter variation on the cell performance.

5.1. Coincident resonances

The transducer/matching layer structure has a clear resonance at 3 MHz visible in Fig. 4, and the fluid layer is also designed to resonate at 3 MHz. However the 3 MHz resonance has disappeared from the full cell (Fig. 5) and effective separation is neither predicted, nor observed at this frequency. This is akin to the classic two degree of freedom vibration absorber problem in which two coincident resonances create two separate peaks with an unexpected null in the response at the individual resonance frequency (see Thomson [13] for example). The phenomenon can also be seen in the model by varying the cavity dimensions around the 3 MHz design frequency.

Fig. 8 shows modelled voltages for resonators with fluid layers having thicknesses corresponding to resonances at 2.6, 2.8, 3.0, 3.2 and 3.4 MHz respectively. In the top graph, quite separate resonances at 2.6 MHz (fluid layer) and 3.0 MHz (transducer/matching layer) can be seen. When the fluid layer resonance is increased to 2.8 MHz, the transducer/matching layer resonance increases in frequency slightly and in the third graph

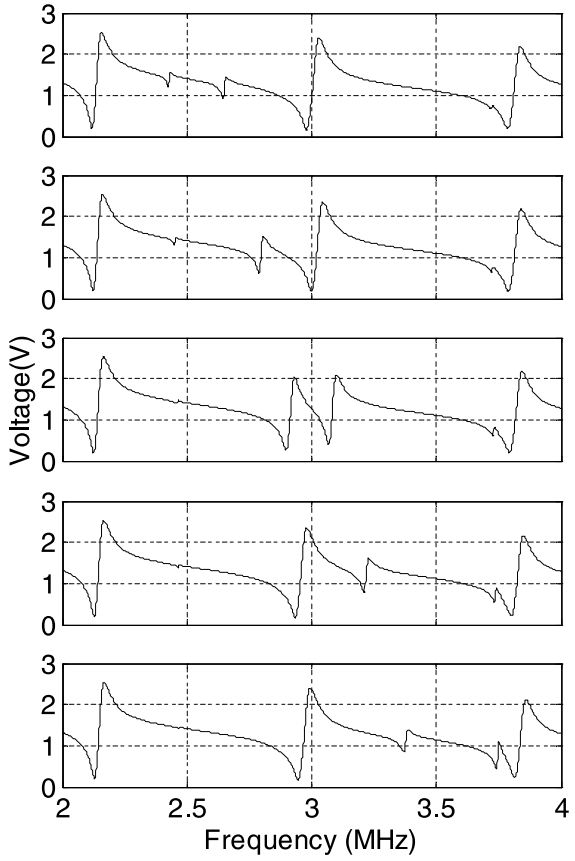

Fig. 8. Input voltage vs frequency for fluid layers with thicknesses corresponding to resonances at (from the top): 2.6, 2.8, 3.0, 3.2 and 3.4 MHz respectively.

(corresponding to the experimental set-up), two coupled resonances either side of three MHz can be seen. By the time the fluid layer resonance has reached 3.4 MHz, the two peaks have re-established themselves at their expected frequencies.

5.2. Pressure profile across the cell

The model is able to predict acoustic pressure profiles across the cell as shown in Fig. 9. The profiles are taken at frequencies that correspond to the modelled peaks of the energy–frequency product (as shown in Fig. 7), at the frequency of the dip between the peaks and at an arbitrary frequency below the peaks.

Only the 3.0 MHz profile corresponds to the classical rigid/rigid boundary acoustic resonance in having the node exactly central and a pressure maximum at the left hand (transducer/matching layer) boundary. The 3.09 MHz standing wave has its maximum pressure to the right of the boundary while the 2.92 MHz standing wave is still rising as the boundary is approached from the right. Hence at these frequencies the impedance offered by the left hand boundary is significantly lower than for a rigid boundary.

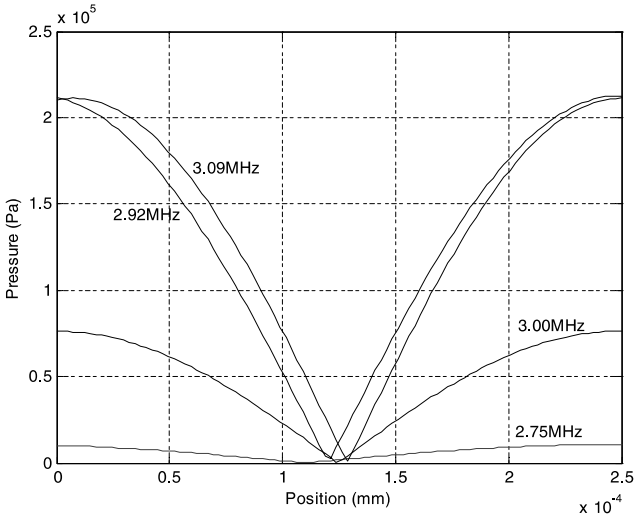

Fig. 9. Pressure amplitudes through fluid layer at following frequencies (in order of decreasing amplitude) 3.09, 2.92, 3.0, and 2.75 MHz.

5.3. Matching layer characteristics

Figs. 10 and 11 model the effect of changing the matching layer thickness. In Fig. 10, the input voltage is shown against frequency for matching layer thicknesses

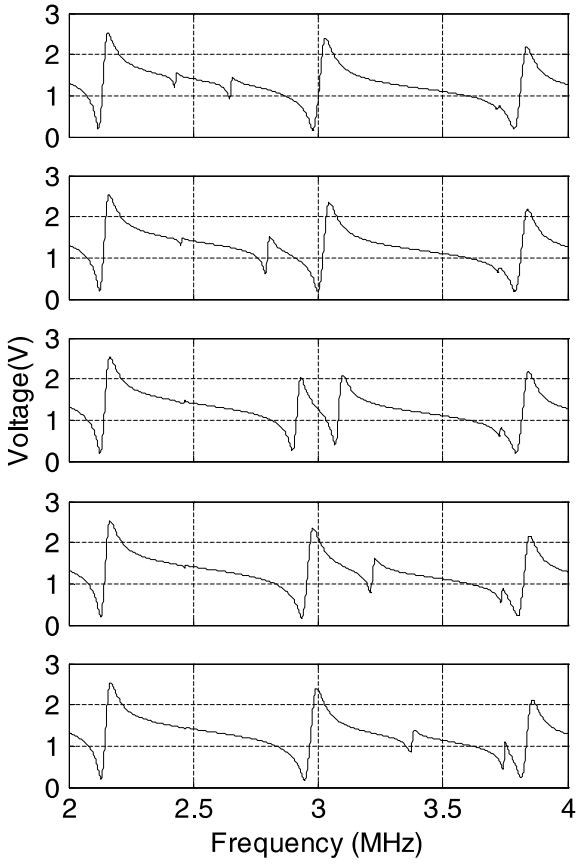

Fig. 10. Modelled input voltage against frequency for different thickness matching layers. From top: no matching layer, then 1/8, 1/4, 1/2, 3/4, and 3/2 λ at 3 MHz respectively.

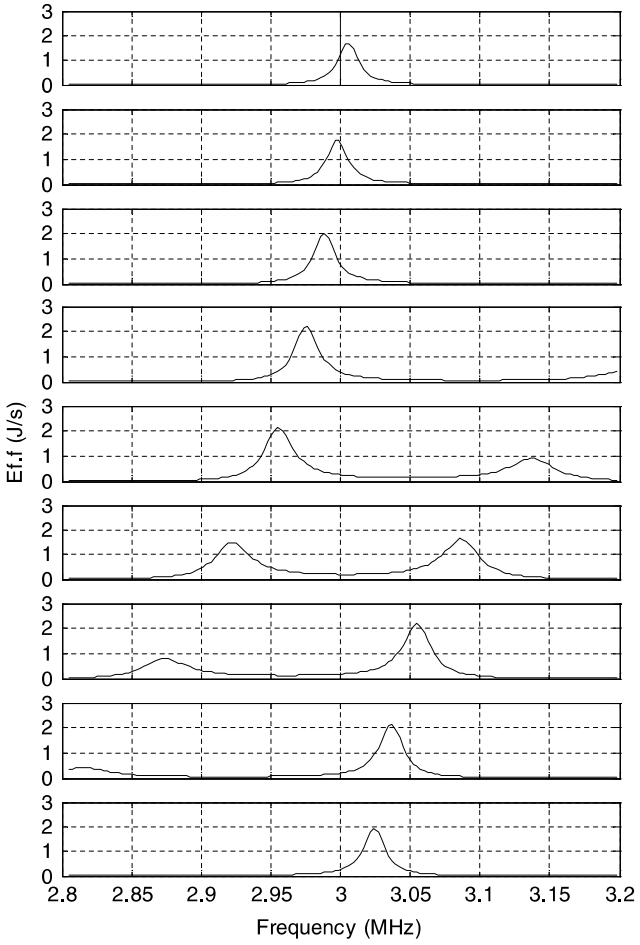

Fig. 11. $E_f f$ vs. frequency for different matching layer thicknesses: from top, 2.6, 2.7, 2.8...3.4 mm respectively.

from 0 to $3/2\lambda$ at 3 MHz (the experimental thickness) in an empty cell. In the top graph, the transducer resonance alone is apparent, and as the matching layer thickness increases, the composite transducer/matching layer resonance frequency decreases due and by the third graph a harmonic of this resonance is visible and by the bottom graph, six harmonics of the composite transducer are visible. In general, these are attributable to the combined transducer and matching layer, and not characteristics of either part alone, although if the bonding between them is not strong (as for the thick adhesive layer example of Fig. 6) individual characteristics become identifiable.

Fig. 11 shows the energy–frequency product against frequency around the working frequency for thicknesses of matching layer close to the design thickness. At 2.6 mm thickness no transducer/matching layer modes are within the frequency range and the 3 MHz fluid layer resonance dominates. This equates to 5/4 wavelengths and the existence of a single peak at odd 1/4 wavelengths has been observed by the authors previously. As the matching layer thickness increases, a transducer/matching layer mode reduces in frequency and starts to force down the 3 MHz resonance (as in the coincident resonance example above). When the transducer/matching layer resonance lies exactly on 3 MHz (graph 6, 3.1 mm thickness) the peaks are split around 3 MHz and the graph is the same as that of Fig. 7. It can be seen that in this design, due to the coincidence of the resonances, small changes in parameters can make a significant difference to the performance characteristics.

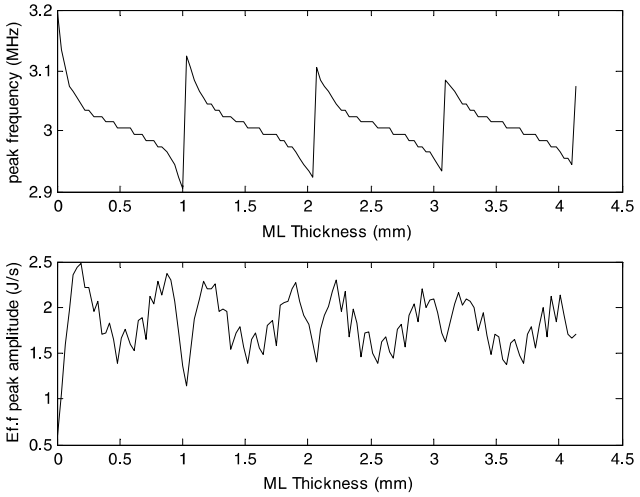

Fig. 12. Variation of the frequency of the energy–frequency product highest peak with matching layer thickness and the magnitude of the peak.

In Fig. 12 the effect of the matching layer thickness on both the frequency and amplitude of the dominant energy–frequency product peak can be seen. At each of the frequencies for which the matching layer is an $n\lambda/2$ resonator the dominant frequency switches from a lower to a higher resonant peak, as was seen in Fig. 11. The behaviour of the peak magnitude is complex, but shows some periodicity with the $\lambda/2$ period. when the transducer/matching layer resonance lies very close to the fluid layer resonance, the pattern of the predicted clearance is very sensitive to small changes in geometric parameters. This may explain the poor prediction of the relative heights of the clearance peaks observed in Fig. 7.

6. Conclusions

It has been shown that the combination of an equivalent-circuit transducer model with impedance and force transfer equations can predict aspects of both the electrical and acoustical behaviour of layered resonator separation cells. Some fine details of behaviour were not predicted by the model, however, perhaps due to the neglect of all but the longitudinal dimension in the model.

In the case where quantitative separation data was available, the product of frequency and stored energy

provided a good indication of where effective separation would occur.

The importance of the adhesive bonding layer has been demonstrated, and it is shown that the model can predict the effects of such a layer.

Modelling of the pressure distribution across the cell has demonstrated how the standing wave at a clearance peak may differ (in terms of nodal position and boundary impedance) from simple, rigid–rigid resonance models.

An examination of the effects of matching layer thicknesses has shown that when the transducer/matching layer resonance lies very close to the fluid layer resonance, the pattern of the predicted clearance is very sensitive to small changes in geometric parameters.

References

[1] M. Gröschl, Ultrasonic separation of suspended particles—Part I: Fundamentals, Acustica 84 (1998) 432–447.
[2] C.J. Schram, Manipulation of particles in an acoustic field, in: T.J. Mason (Ed.), Advances in Sonochemistry, 1991.
[3] W.T. Coakley, Ultrasonic separations in analytical biotechnology, Trends in Biotechnology 15 (1997) 506–511.
[4] M. Hill, R.J.K. Wood, Modelling in the design of a flow-through ultrasonic separator, Ultrasonics 38 (2000) 662–665.
[5] M. Hill, The use of ultrasonics to concentrate particles within a low flow-rate fluid, in: MTEC International Conference on Sensors & Transducers, Birmingham, UK, 2000.
[6] H. Nowotny, E. Benes, General one-dimensional treatment of the layered piezoelectric resonator with 2 electrodes, J. Acoust. Soc. Am. 82 (1987) 513–521.
[7] Stansfield, Underwater Electroacoustic Transducers—A Handbook for Users and Designers, Bath University, Bath, 1990.
[8] T. Hueter, R. Bolt, Sonics: techniques... in engineering & science, 1955.
[9] L.E. Kinsler, A.E. Frey, A.B. Coppens, J.V. Sanders, Fundamentals of Acoustics, Wiley, New York, 1982.
[10] T.L. Tolt, D.L. Feke, Separation of dispersed phases from liquids in acoustically driven chambers, Chem. Eng. Sci. 48 (1992) 527–540.
[11] M. Gröschl, Ultrasonic separation of suspended particles—Part II: Design and operation of separation devices, Acustica 84 (1998) 632–642.
[12] J.J. Hawkes, W.T. Coakley, Force field particle filter, combining ultrasound standing waves and laminar flow, Sensor. Actuat. B-Chem. 75 (2001) 213–222.
[13] W.T. Thomson, Theory of Vibration with Applications, Unwin, London, 1988.